Asian Journal of Chemistry; Vol. 38, No. 5 (2026), 1159-1169
ASIAN JOURNAL OF CHEMISTRY
https://doi.org/10.14233/ajchem.2026.35505

Heterogenous Photocatalytic Degradation of Sugarcane Distillery Spent Wash by using Mesoporous Zn-TiO_2 Catalyst

AMOL S. BHOSALE[1,*], NETAJI P. MALI[1], SHAILA B. DHOTRE[1], SHRIKANT P. TAKLE[1], AARTI S. WARE[2], RAVINDRA U. MENE[3] and NAMDEO N. BHUJBAL[1]

[1]Department of Chemistry, Annasaheb Magar Mahavidyalaya, Hadapsar, Pune-411028, India
[2]MAEER's MIT Saint Dnyaneshwar College, Pune-412105, India
[3]Department of Physics, Annasaheb Magar Mahavidyalaya, Hadapsar, Pune-411028, India

*Corresponding author: E-mail: amolbhosale4141@gmail.com

Received: 23 December 2025 *Accepted*: 12 March 2026 *Published online*: 4 May 2026 AJC-22340

Sugarcane distillery spent wash is a highly coloured wastewater that requires efficient treatment. In this study, Zn-doped TiO_2 (1-5 wt.%) photocatalysts were synthesized by a sol-gel method and applied for sunlight-driven degradation of spent wash. XRD confirmed phase-pure anatase TiO_2, while the absence of ZnO peaks indicated successful Zn^{2+} incorporation into the TiO_2 lattice. FE-SEM, HR-TEM and elemental mapping revealed nanosized particles with uniform Zn distribution. Among all samples, 4% Zn-TiO_2 showed the highest surface area (116 $m^2 g^{-1}$) compared with undoped TiO_2 (80 $m^2 g^{-1}$). UV-DRS analysis showed band-gap reduction from 3.09 eV to 2.93 eV, while photoluminescence studies indicated suppressed electron-hole recombination. Under natural sunlight, 4% Zn-TiO_2 exhibited the best photocatalytic performance, achieving 78% colour removal within 6 h, compared with 62% for pure TiO_2. The degradation followed pseudo-first-order kinetics with the highest rate constant (0.00506 min^{-1}). The optimized catalyst also achieved 72% COD and 65% TOC removal, confirming effective mineralisation of pollutants. After four reuse cycles, the catalyst retained over 73% activity, demonstrating good stability. The enhanced performance of 4% Zn-TiO_2 is attributed to higher surface area, reduced band gap, improved charge separation and stable anatase structure, making it a promising reusable photocatalyst for sustainable distillery wastewater treatment.

Keywords: Spent wash, Photocatalysis, Sugar industry wastewater, Zn doped TiO_2.

INTRODUCTION

The distillery industry, which makes ethyl alcohol from sugarcane molasses, produces high volumes of wastewater referred to as distillery spent wash (DSW). For each litre of alcohol produced around 12-15 litres of spent wash are produced [1]. In India, nearly 40 billion litres of this wastewater are generated annually [2]. Spent wash is a dark brown, foul-smelling, acidic effluent with high COD and BOD levels. Its colour mainly arises from melanoidins generated through Maillard reactions between sugars and amino acids [3]. These are non-biodegradable and environmentally toxic substances along with phenolics, lignin derivatives, sulphates and heavy metals [4]. Untreated distillery spent wash discharged into rivers causes water deoxygenation, damages aquatic life and poses serious health risks [5].

Distillery spent wash has been treated by several conventional methods; however, each approach has significant limitations. The biological processes such as anaerobic digestion can reduce biodegradable organic load, but they are generally ineffective for colour removal because melanoidins and other high molecular-weight compounds are resistant to microbial degradation [6]. The physico-chemical methods including coagulation, flocculation, activated carbon adsorption and membrane filtration provide only partial decolourisation, while also involving high operational costs and generation of secondary sludge [7]. Advanced treatments such as ozonation and electrochemical oxidation are efficient, yet their high energy and chemical requirements restrict large-scale application [8]. These drawbacks underline the need for sustainable and cost-effective alternatives.

Advanced oxidation processes (AOPs) have emerged as promising technologies for wastewater remediation because they generate highly reactive hydroxyl radicals capable of oxidizing persistent organic pollutants into simpler end products such as water and carbon dioxide [9]. Among these, semi-

This is an open access journal, and articles are distributed under the terms of the Attribution 4.0 International (CC BY 4.0) License. This license lets others distribute, remix, tweak, and build upon your work, even commercially, as long as they credit the author for the original creation. You must give appropriate credit, provide a link to the license, and indicate if changes were made.

conductor photocatalysis has received considerable attention since it operates under mild conditions, can utilize solar energy and generally requires no additional chemical reagents [10].

Titanium dioxide (TiO_2) is one of the most widely studied photocatalysts owing to its chemical stability, strong oxidizing ability, low toxicity and affordability [11]. It has shown excellent potential in degrading dyes, pesticides, and pathogenic contaminants [12]. Nevertheless, TiO_2 suffers from two inherent limitations. First, anatase TiO_2 possesses a band gap of about 3.2 eV, allowing absorption mainly in the UV region, which represents only a small fraction of solar radiation. Second, rapid recombination of photogenerated electron-hole pairs significantly lowers its photocatalytic efficiency [13,14].

To overcome these limitations, several modification strategies have been explored, including dye sensitization, coupling with other semiconductors, surface engineering and doping with metal or non-metal elements [15-17]. Although dye sensitization improves visible-light response, the dyes often suffer from photodegradation [18]. Semiconductor coupling systems such as CdS/TiO_2 can enhance activity but may raise toxicity concerns [19]. Non-metal doping using nitrogen, carbon, sulphur or phosphorus can extend light absorption, though dopant stability is often limited [20-23]. In contrast, metal ion doping has proven particularly effective because it can introduce intermediate energy states, enhance visible-light harvesting and suppress charge recombination [24]. Various metals such as Fe, Cu, Cr, V, Ni and Co have been investigated [11,20,25-29], but some exhibit toxicity, instability or recombination-related drawbacks [30-33].

Among these dopants, zinc has attracted increasing interest. The ionic radius of Zn^{2+} is comparable to that of Ti^{4+}, allowing substitution within the TiO_2 lattice with minimal structural distortion [34]. Zn incorporation can create shallow donor levels, reduce band-gap energy, improve charge mobility and increase surface hydroxylation, all of which are beneficial for photocatalysis [35]. Moreover, Zn-doped TiO_2 often exhibits lower photoluminescence intensity than pristine TiO_2, indicating reduced electron-hole recombination [36]. Zinc is also more environmentally benign than several transition-metal dopants such as chromium or vanadium [37,38]. Previous studies have demonstrated the effectiveness of Zn-doped TiO_2 for degradation of dyes and phenolic pollutants under visible light [39].

Despite these advantages, only limited studies have examined Zn-doped TiO_2 for treatment of real industrial effluents such as distillery spent wash, which is far more complex than model dye solutions. The synthesis route strongly influences the structural and catalytic properties of doped-TiO_2. Hydrothermal methods offer high crystallinity but require elevated pressure and long reaction times [29,40]. Coprecipitation is simple but may lead to poor dopant dispersion [41]. Techniques such as sputtering or ion implantation provide precise doping control but are expensive and unsuitable for bulk production [42]. In comparison, the sol-gel method is versatile, economical and capable of producing homogeneous nanoparticles with controlled particle size, porosity and uniform dopant distribution [43,44]. It also facilitates effective incorporation of Zn without phase separation at suitable concentrations [45].

Accordingly, the present study focuses on the synthesis of Zn-doped TiO_2 nanoparticles by a sol-gel route and their application in solar-light-driven degradation of distillery spent wash. This study mainly examines the influence of Zn doping on band-gap reduction, charge separation, surface properties, and photocatalytic efficiency. By testing the catalyst on real industrial effluent instead of model pollutants, this work offers useful insight for sustainable wastewater treatment in the distillery industry.

EXPERIMENTAL

The chemicals and solvents were used for the synthesis of Zn-TiO_2 catalysts without further treatment/purification. Titanium tetraisopropoxide (TTIP, $C_{12}H_{28}O_4Ti$, 97%, obtained from Sigma-Aldrich), hydrogen peroxide (H_2O_2, 30% w/v, Merck India Ltd.), zinc nitrate hexahydrate ($Zn(NO_3)_2{\cdot}6H_2O$, 98%, Merck India Ltd.) were used as precursors for synthesis. Milli-Q water (conductivity 0.06 μS cm^{-1}, Q-Pad filter system) was used for the solution preparations.

Synthesis of catalysts: The synthesis of TiO_2 was carried out by using a simple, cost-effective sol-gel method [27,46]. In this synthesis, 7.1 mL of TTIP was added to 100 mL of milli-Q water under constant stirring at room temperature for 0.5 h. A white titanium hydroxide precipitate was formed through hydrolysis and allowed to settle for 1 h. The supernatant was decanted, and the precipitate was washed with Milli-Q water to remove residual alcohol. Subsequently, 30 mL of hydrogen peroxide (30% w/w H_2O_2) was added slowly under stirring, resulting in the formation of an orange titanium peroxide sol. On standing at room temperature, the sol gradually converted into a thick gel. The obtained gel was dried at 105 ºC and then calcined at 400 ºC.

For the synthesis of Zn-doped TiO_2, the same procedure was followed to obtain a transparent orange sol. An appropriate amount of $Zn(NO_3)_2{\cdot}6H_2O$ (1-5 wt.%), dissolved in Milli-Q water and hydrogen peroxide, was added slowly under constant stirring. The resulting mixture gradually transformed into a thick viscous gel, which was dried at 105 ºC and subsequently annealed at 400 ºC. The calcination temperature was selected based on TGA results.

Characterisation: The crystallographic structure of prepared sample was analysed by using Rigaku Ultima IV X-ray diffractometer (Cu*K*α radiation as a radiation source) (λ = 1.5406 Å) and the diffraction data was collected in the 2θ range of 5-80º at a scan rate of 0.02º min^{-1}. Morphological analysis and elemental composition of the catalysts was carried out using a field emission scanning electron microscope (FE-SEM, Nova NanoSEM NPEP303). Along with this distribution of Zn over the TiO_2 was carried out by using energy dispersive X-ray spectroscopy (EDX) supported with essential mapping study. In addition, TEM images were attained using a PHILIPS CM200 field emission transmission electron microscope (FE-TEM) with operating voltages of 20-200 kV and a resolution of 2.4 Å along with this selected area electron diffraction (SAED) were also recorded. The chemical state of the material was investigated using XPS spectroscopy (Thermo fisher Scientific). Functional groups investigation was done by using Fourier transform infrared (FTIR) spectroscopy. The

FTIR spectrum were recorded using a Two U-ATR Perkin-Elmer instrument in the transmission mode over a range of 4000-450 cm^{-1}. The optical properties of sample were analysed by using Perkin Elmer UV-Visible spectrophotometer over a range of 200-800 nm. The separation of photo-generated electron-hole pair and the recombination efficiency of synthesised material was recorded by using a FP-8300 Spectrophotometer. Raman spectroscopy was used to investigate the vibrational properties and crystalline structure of the undoped and doped TiO_2 by using HORIBA Scientific with laser wavelength 425 nm as an excitation source. The uncalcined powder in the sol-gel method was subjected to thermal decomposition using SDT Q600 V20.9 Build 20 equipment. The temperature was increased from room temperature to 1000 ºC at a heating rate of 10 ºC min^{-1} and α-Al_2O_3 was used as the reference.

Photocatalytic decomposition of spent wash colour: The photocatalytic activity of the synthesised catalyst was examined for the colour degradation of cane sugar distillery wastewater called as spent wash or vinasse under natural sunlight. For this study, aqueous solution of spent wash (2500 ppm) was prepared. For each set, a 100 mL of aqueous solutions of spent wash was taken in 250 mL glass beaker with 50 mg of undoped and Zn-doped (1-5%) TiO_2 catalyst. To establish adsorption-desorption equilibrium, the suspension was kept in the dark for 1 h. The photocatalytic experiments were conducted under natural sunlight between 10:00 am and 4:00 p.m. at Pune, India. The average solar intensity during the experiments was approximately 1120W m^{-2}, measured using a calibrated digital solar power meter. The experiments were performed under clear sky condition. Direct sunlight has a luminous efficacy of ~93 lumens per watt radiant flux. Small aliquots of the mixture were removed at regular intervals during irradiation and allowed to settle for 20 min. The supernatant solution was then analysed by UV-Vis spectrophotometer. The percent mineralisation of the spent wash was determined by colour degradation.

RESULTS AND DISCUSSION

Thermogravimetric studies: The thermogravimetric (TG) curve (Fig. 1) shows the weight loss of the uncalcined 1% Zn-TiO_2 sample. The curve has three clear stages of weight loss. The stable region confirms the formation of crystalline Zn-TiO_2 nanoparticles. The sample loss around 25% of its total weight, which shows that volatile and organic parts are completely removed on heating. The TGA results suggest that calcination above 400 ºC is enough to obtain a undoped and stable Zn-TiO_2 nanocatalyst suitable for photocatalytic use.

XRD studies: The XRD patterns of undoped and Zn-doped TiO_2 catalysts with varying Zn content (1-5 wt. %) calcined at 400 ºC are presented in Fig. 2a-f. All the diffraction peaks are referenced to anatase phase TiO_2 (JCPDS No. 21-1272) with typical reflections at $2\theta \approx 25.3^o$, 37.8^o, 48.0^o, 53.9^o, 55.1^o and 62.7^o, corresponding to the (101), (004), (200), (105), (211) and (204) lattice planes, respectively [47,48]. The absence of a diffraction peak at $2\theta = 30.7^o$ indicates no brookite phase formed at that temperature. The pattern of undoped TiO_2 (a) exhibits sharp and intense peaks, indicating high crystallinity. Upon doping with Zn (Fig. 2b-f), no secondary phases

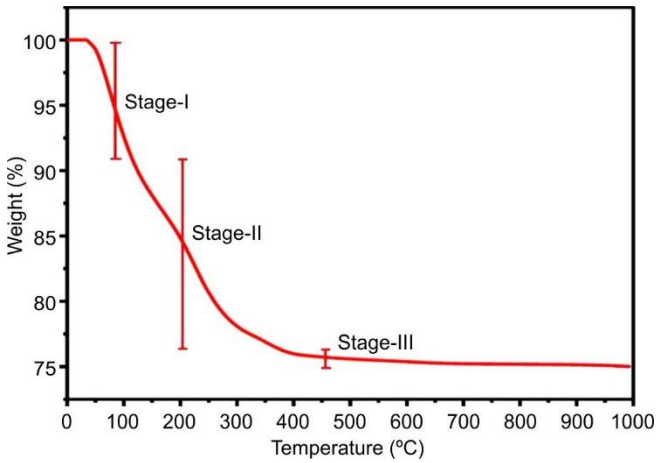

Fig. 1. TGA curve of 1% Zn-TiO_2 powdered gel sample

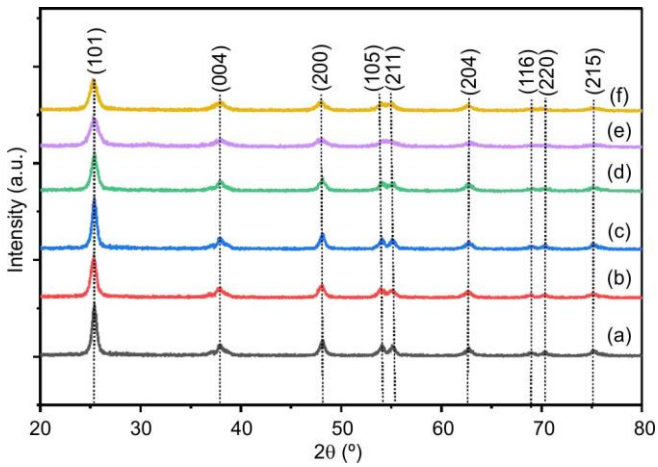

Fig. 2. XRD patterns of (a) undoped TiO_2, (b) 1% Zn-TiO_2, (c) 2% Zn-TiO_2, (d) 3% Zn-TiO_2, (e) 4% Zn-TiO_2 and (f) 5% Zn-TiO_2 calcined at 400 ºC

such as Zn or ZnO were observed, even at the highest doping level of 5%, suggesting successful incorporation of Zn^{2+} into the TiO_2 lattice without forming separate phases. A gradual decrease in peak intensity and slight peak broadening with increasing Zn content suggest a reduction in crystallite size and increased lattice distortion.

BET studies: Prior to BET measurement the sample were degassed with N_2 at 90 ºC for 1 h and then 120 ºC for 3 h. The isotherm was logged at 77 K by using LN2 on Nova Quantachrome Touch Win V1.24 instrument. The BET isotherm for Zn-TiO_2 sample is shown in Fig. 3. The mesoporous Zn doped TiO_2 exhibit Type-IV isotherm curves with H_2 type hysteresis loop represent the capillary condensation in so called ink-bottle shaped pores *i.e.* having an entrance diameter smaller than the size of the pore body. The surface area measurements are reasonably remarkable as undoped TiO_2 shows surface area of 80 m^2 g^{-1}, whereas 4% Zn-TiO_2 shows higher surface area 116 m^2 g^{-1} as compared to other concentrations. The surface area value of all Zn doped sample is depicted in Table-1. The surface area depends on the particle size, pore size, number and type of pores and distribution of pores with voids.

FE-SEM studies: Fig. 4 shows the scanning electron microscopy (SEM) image of undoped TiO_2 and 4% Zn-doped TiO_2 particles, which provides a visual representation of the

TABLE-1
COMPARATIVE SUMMARY OF PHYSICO-CHEMICAL AND PHOTOCATALYTIC PROPERTIES OF Zn-DOPED TIO_2 SAMPLES

Sample	Surface area (m^2/g)	Band gap (eV)	PL intensity (a.u.)	Rate constant, k (min^{-1})	Degradation efficiency (%)
TiO_2	80	3.09	510	0.00323	62
1% Zn-TiO_2	84	3.00	465	0.00350	65
2% Zn-TiO_2	91	3.05	415	0.00391	69
3% Zn-TiO_2	97	3.02	395	0.00438	73
4% Zn-TiO_2	116	2.93	310	0.00506	78
5% Zn-TiO_2	103	2.97	340	0.00463	75

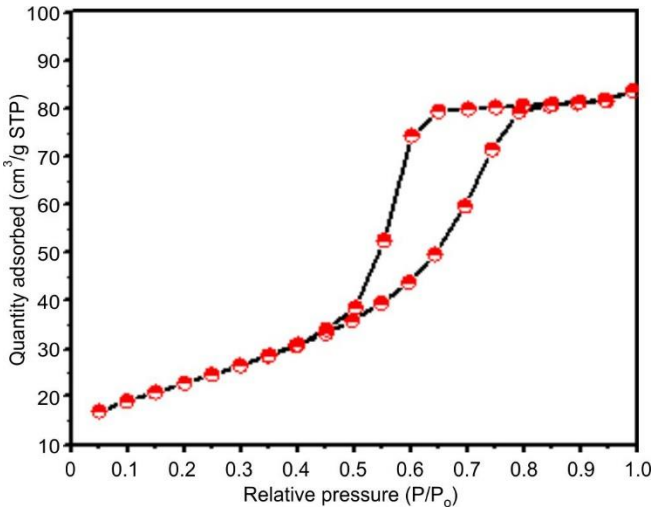

Fig. 3. Nitrogen adsorption-desorption isotherms (BET analysis) of 4% Zn-TiO_2

particle distribution of both the samples. The nanopowder exhibits a uniform spherical morphology of the particles. However, some degree of agglomeration is also observed in the both samples. The EDAX patterns of the TiO_2 and 4% Zn-TiO_2 samples are shown in Fig. 4c-d. These patterns confirm the presence of Zn within the titania NPs and provide information to determine the elemental composition of the material. The patterns confirm the presence of Ti, Zn and O elements in all doped samples. Also, no unwanted elemental peaks are observed, which indicates purity of the synthesised samples. The elemental mapping image (Fig. 5) indicate the distribution of Ti, O and Zn across the sample surface. The Zn spots, marked in red in the mapping image are uniformed spread in the scanned region. This uniform distribution of Zn proves that doping occurs homogenously and no formation of Zn rich cluster. Such proper mixing helps in better charge separation during photocatalysis.

FE-TEM studies: High-resolution transmission electron microscopy (HR-TEM) analysis technique was used to find the crystallinity, particle size and phase structure of the catalysts. Fig. 6 depicts HR-TEM image of 4% Zn doped TiO_2 nanoparticles. The particles size was found to be ~ 10-25 nm. The 4% Zn-TiO_2 nanocatalyst showing clear lattice fringes corresponding to the (101) plane of anatase, with a *d*-spacing of about 0.35 nm. This type of lattice fringes, indicating that the

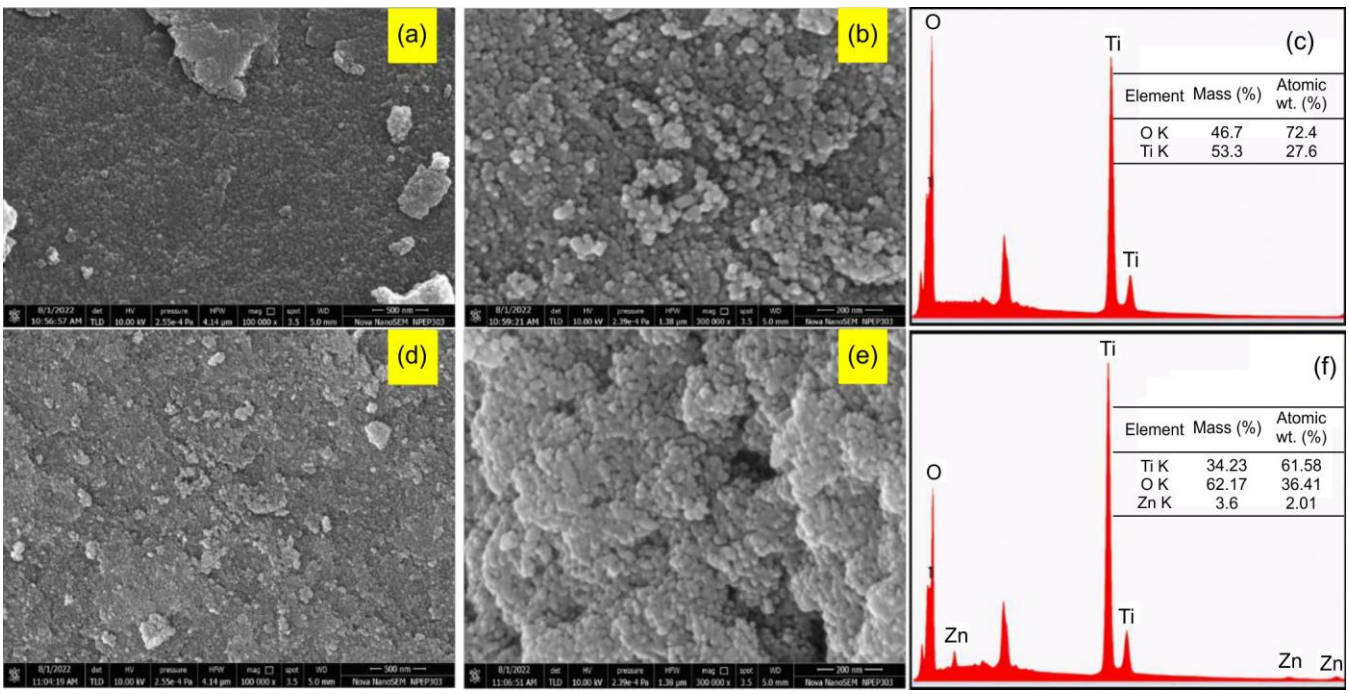

Fig. 4. FESEM images of (a & b) low and high magnification image of TiO_2 and (d & e) low and high magnification image of 4% Zn-TiO_2, (c & f) EDAX patterns of TiO_2 and 4% Zn-TiO_2, respectively

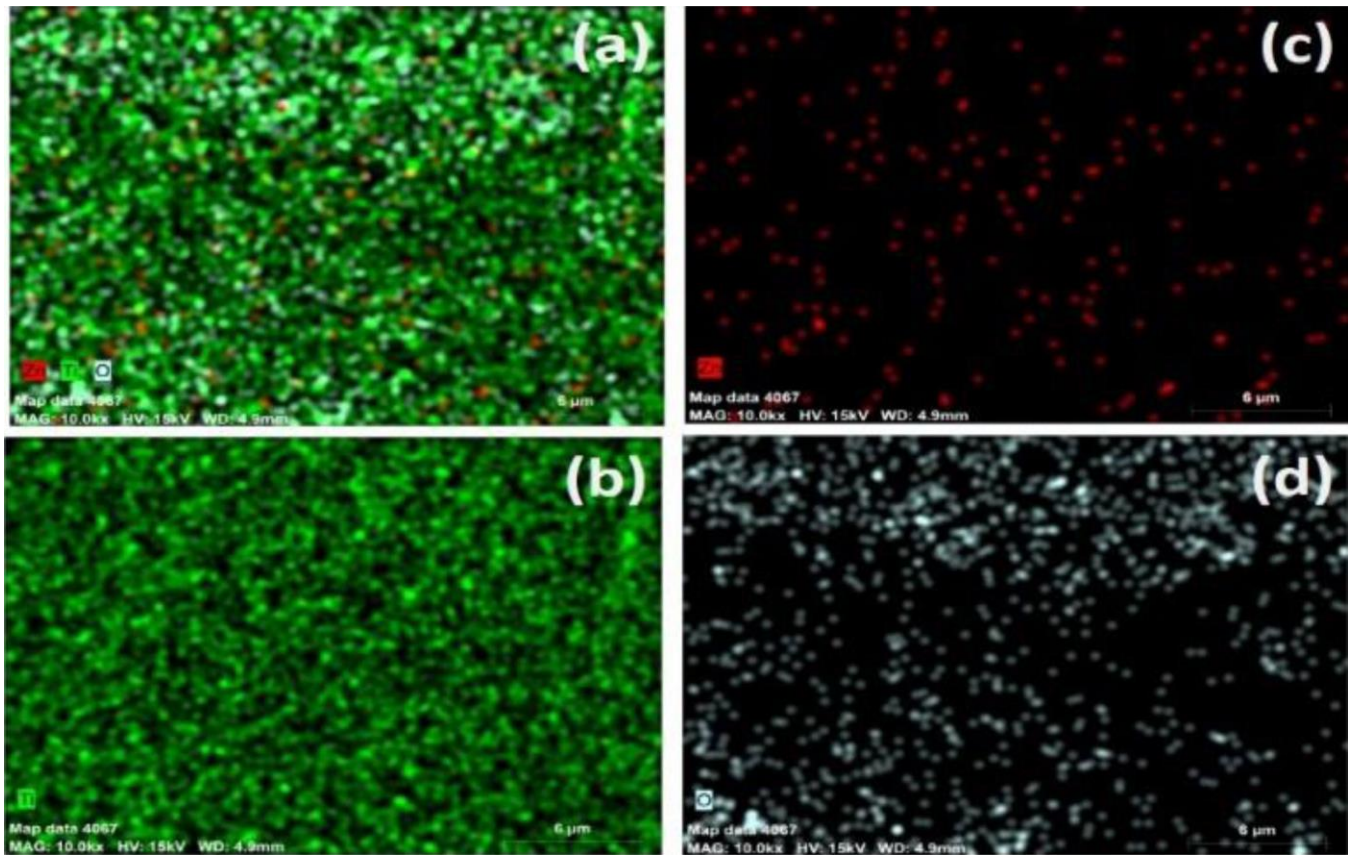

Fig. 5. FESEM elemental mapping of 4% Zn-TiO_2 catalyst: (a) Zn, Ti & O (b) Ti, (c) Zn and (d) O

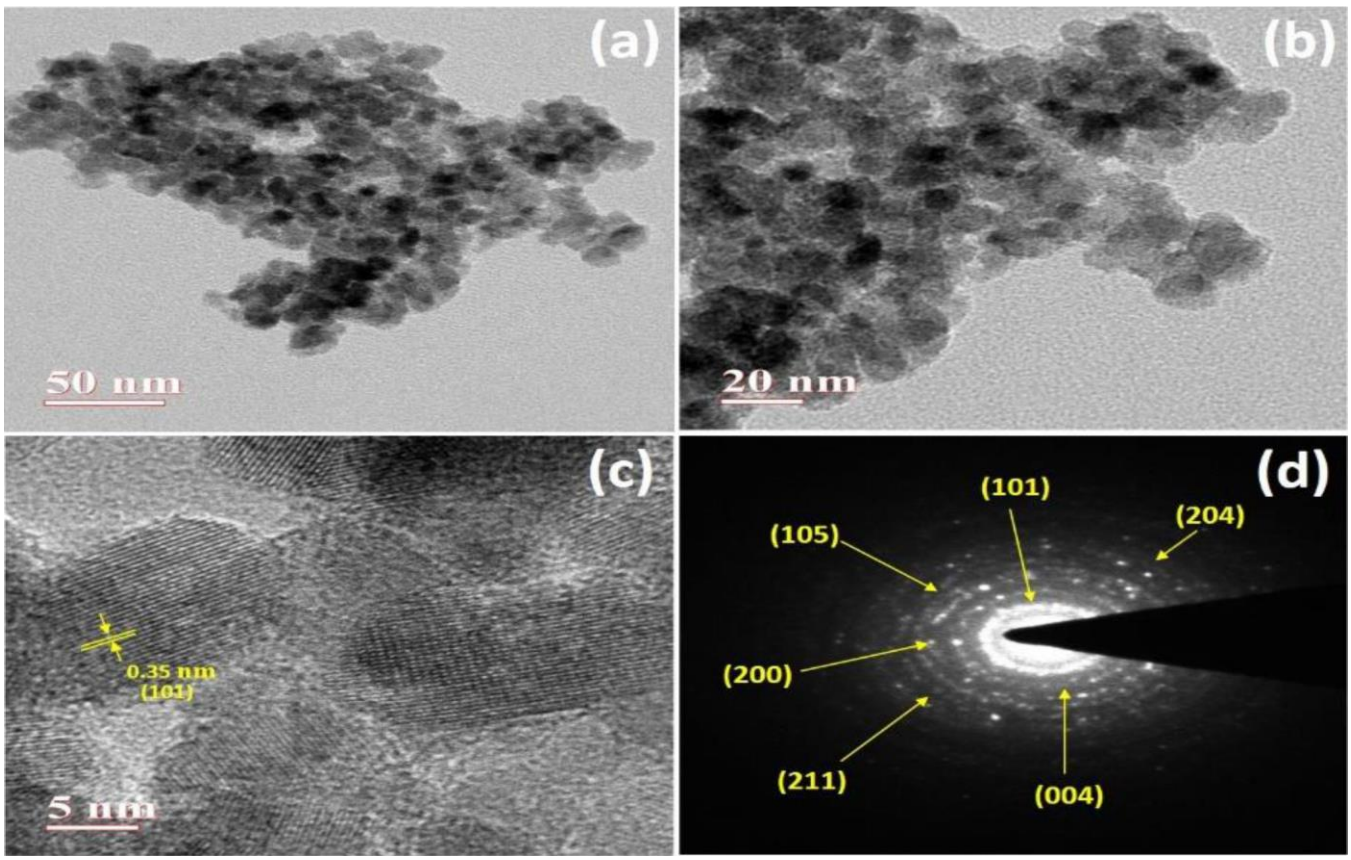

Fig. 6. TEM images of 4% Zn-TiO_2 samples, (a) & (b) low magnification (c) high magnification (d) SAED pattern of 4% Zn-TiO_2

incorporation of Zn does not disrupt the anatase crystal structure. Selected area electron diffraction (SAED) pattern of 4% Zn-TiO_2 sample in Fig. 6d showed concentric rings, which were found to be associated with the characteristic planes of anatase TiO_2. No lattice fringes or diffraction rings related to ZnO or any other secondary phases were found in the doped sample. This suggests that the Zn^{2+} ions were successfully incorporated into the TiO_2 lattice structure without forming separate ZnO clusters. The retained crystallinity and phase purity indicate that the sol-gel synthesis method effectively achieved a uniform incorporation of the dopant.

FT-IR studies: The FTIR spectra of undoped and Zn-TiO_2 samples annealed at 400 ºC were measured in the range 4000-450 cm^{-1}. The thermogram indicates typical absorption bellow ~700-600 cm^{-1} related to Ti-O and Ti-O-Ti lattice vibrations (Fig. 7). It ensuring that the TiO_2 network remain as it is after Zn incorporation. The reduction of transmittance with Zn content increase in undoped and (1-5 wt. %) Zn-TiO_2 indicates enhanced lattice disorder, phonon scattering and oxygen vacancy related defects caused by Zn doping. Lack of new Zn-O bands at 450-430 cm^{-1} corresponding to vibrations of Zn-O beyond the Ti-O regime confirms that Zn is incorporated in the TiO_2 lattice instead of forming a ZnO phase.

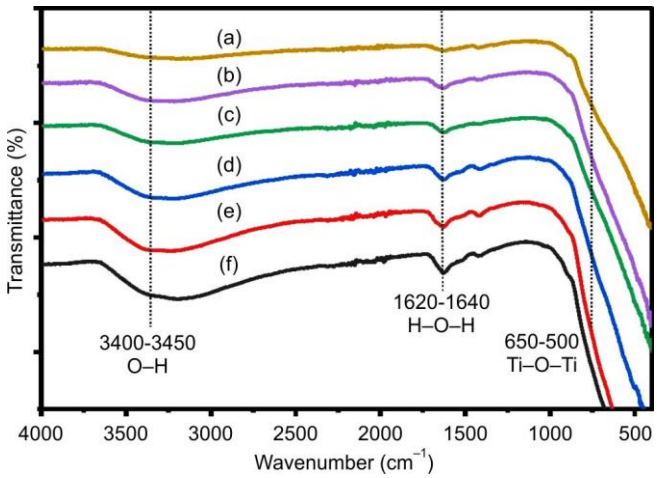

Fig. 7. FT-IR spectra of (a)TiO_2, (b) 1% Zn-TiO_2, (c) 2% Zn-TiO_2, (d) 3% Zn-TiO_2, (e) 4% Zn-TiO_2 and (f) 5% Zn-TiO_2 calcined at 400 ºC

Raman spectral studies: The Raman spectra of undoped TiO_2 and 4% Zn-doped TiO_2 are shown in Fig. 8. The undoped TiO_2 shows usual anatase peaks at approximately 145 cm^{-1} (E_g), 398.20 cm^{-1} (B_{1g}), 520.82 cm^{-1} (A_{1g} + B_{1g}) and 639.58 cm^{-1} (E_g) and 4 % Zn-TiO_2 Shows peak at 147 cm^{-1} (E_g),

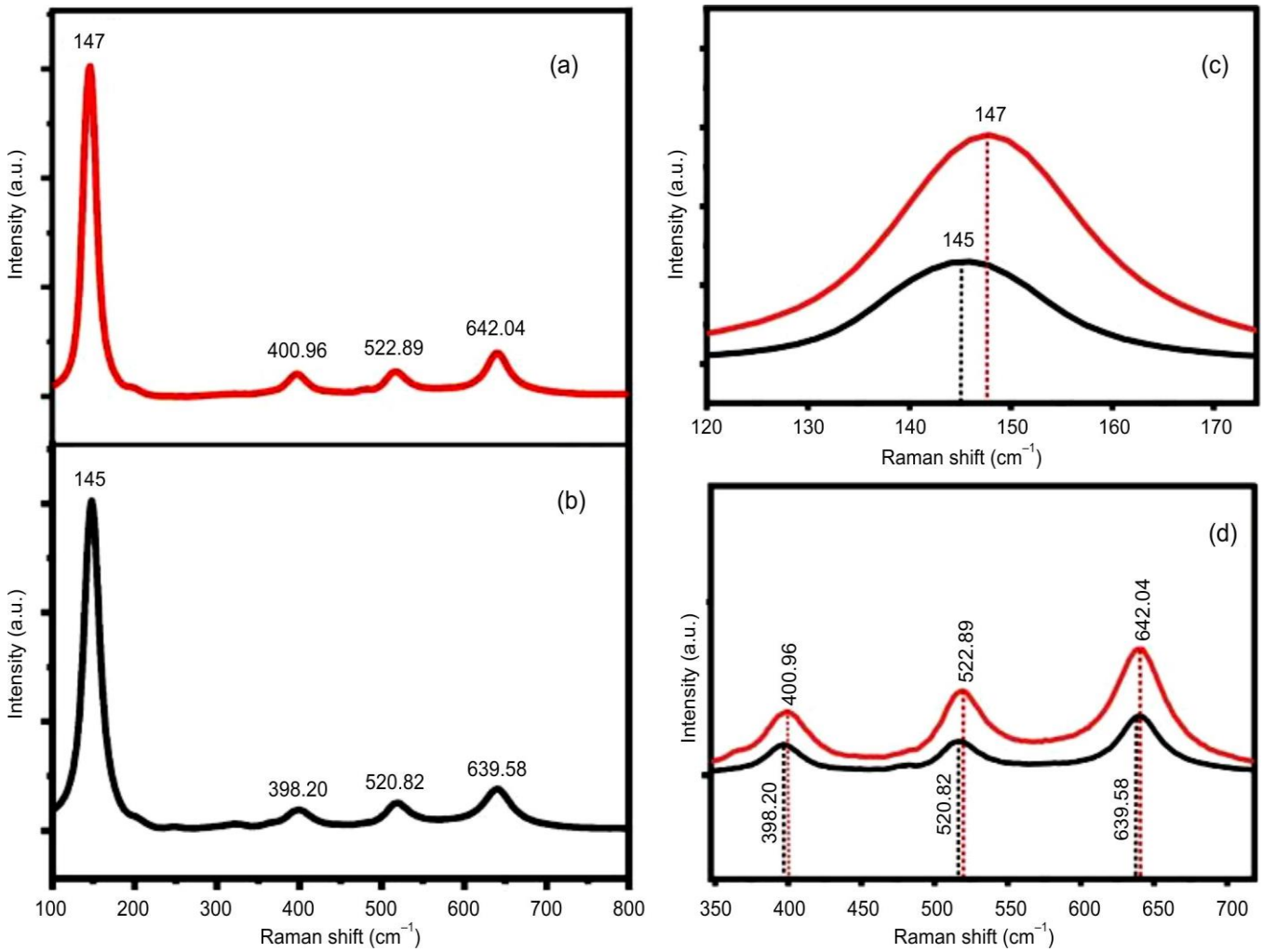

Fig. 8. Raman spectra of (a) 4% Zn-TiO_2, (b) undoped TiO_2 sample and (c) & (d) Raman shifts

400.96 cm^{-1} (B_{1g}), 522.89 cm^{-1} (A_{1g} + B_{1g}) and 642.04 cm^{-1} (E_g), thus confirmed the anatase phase after Zn incorporation. The peak with the maximum E_g at 145 cm^{-1} was broadened and shifted slightly to around 147 cm^{-1}. The peak broadening and slight shift indicate lattice distortion and oxygen vacancy formation, arising from partial substitution of Ti^{4+} ions in the TiO_2 lattice by Zn^{2+} ions. There was no indication of peaks of rutile and brookite phases and thus the phase purity was confirmed.

XPS analysis: XPS survey spectra (Fig. 9) confirmed the presence of Ti, O and Zn in the Zn-doped TiO_2 samples, along with surface contaminant carbon (C 1s). The clear Zn signal in the doped samples indicates successful incorporation of Zn into the TiO_2 matrix. The clear Zn signal in the doped sample confirms successful Zn incorporation. The high-resolution Ti 2p spectrum of undoped TiO_2 showed characteristic doublet peaks at 457.8 eV (Ti $2p_{3/2}$) and 463.7 eV (Ti $2p_{1/2}$), corresponding to Ti^{4+} in the anatase lattice. In Zn-doped TiO_2, these peaks shifted slightly to higher binding energies (458.3 and 464.2 eV), indicating changes in the chemical environment of Ti after Zn incorporation. The Zn 2p spectrum displayed peaks at 1021.5 eV (Zn $2p_{3/2}$) and 1044.6 eV (Zn $2p_{1/2}$), confirming the presence of Zn^{2+} within the TiO_2 matrix.

Photoluminescence (PL) studies: The PL spectra of undoped and Zn-doped TiO_2 with different doping levels (1-5 wt.%) were measured at an excitation wavelength of 425 nm. All the samples have an intense emission peak at around 425 nm corresponding to near-band-edge (NBE) emission as a result of direct VB-to-CB transitions (Fig. 10). Along with this, broad weak emissions between 450-550 nm can be assigned to defect-related states in Zn-doped TiO_2. On comparing the spectra, Zn-doped sample shows lower PL intensity in comparison with undoped TiO_2, indicating most efficient suppression of electron-hole recombination and enhanced charge carrier separation. it is confirmed that 4% Zn-TiO_2 shows the lowest PL intensity, which suggesting that the most efficient suppression of electron-hole recombination and higher charge carrier separation. This quenching occurring due to the introduction of Zn^{2+} ions as electron traps in the host TiO_2 lattice, generating charge separation and increasing photogenerated carrier lifetimes.

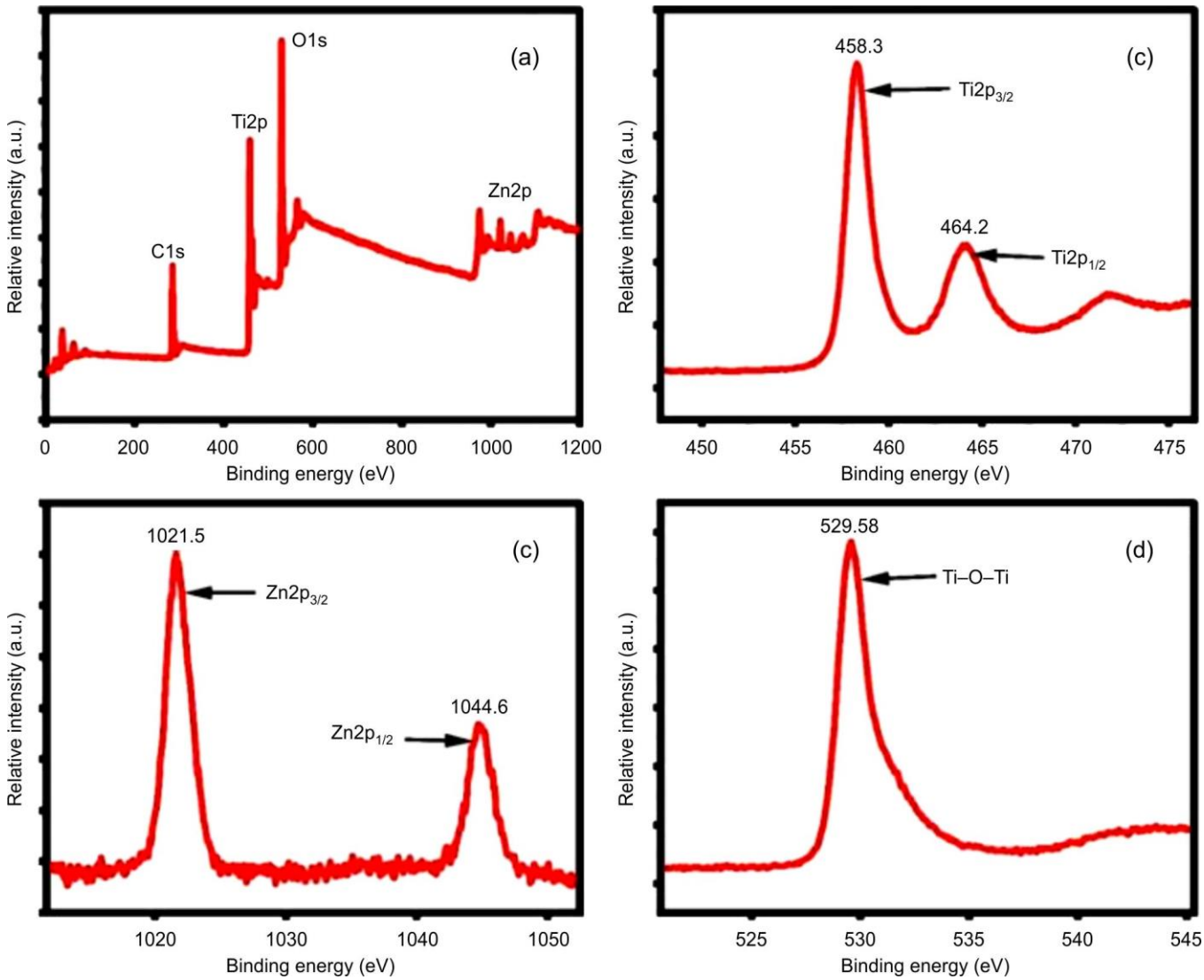

Fig. 9. XPS spectra of 4% Zn-TiO_2 catalyst (a) XPS survey, (b)Ti 2p spectrum, (c) Zn 2p spectrum and (d) O 1s spectrum

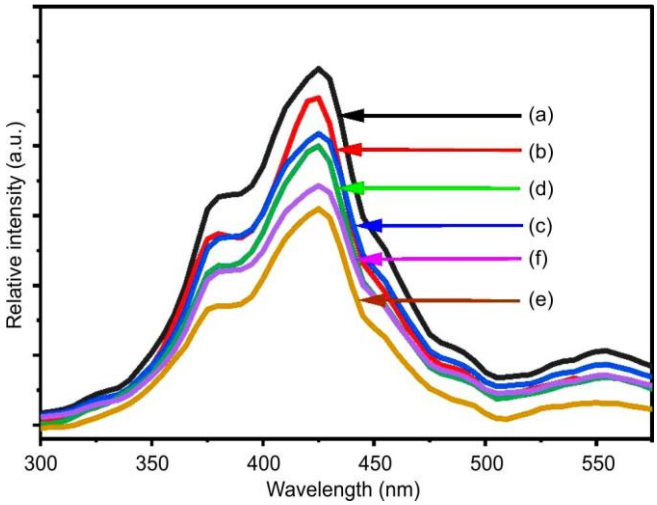

Fig. 10. PL spectra of samples calcined at 400 ºC: (a) TiO_2, (b) 1% Zn-TiO_2 and (c) 2% Zn-TiO_2 (d) 3% Zn-TiO_2 (e) 4% Zn-TiO_2 and (f) 5% Zn-TiO_2

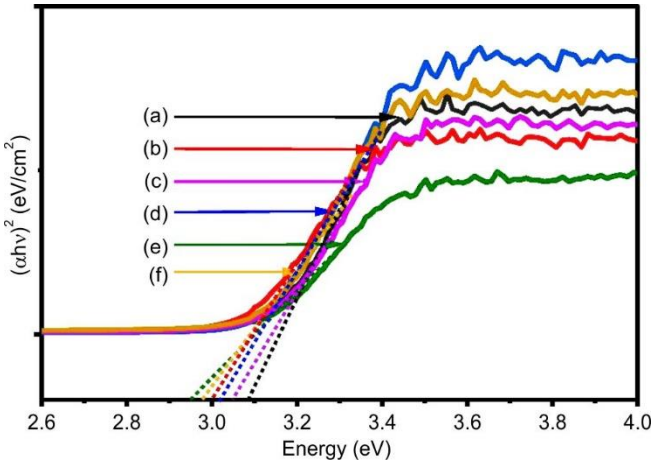

Fig. 11. Tauc plots for (a) TiO_2, (b) 1% Zn-TiO_2, (c) 2% Zn-TiO_2, (d) 3% Zn-TiO_2, (e) 4% Zn-TiO_2 and (f) 5% Zn-TiO_2

UV-DRS studies: The band gap for all the catalysts were determined using a Tauc plot indicate that there has been a substantial decrease in band gap energy for Zn doped samples. In undoped TiO_2, there was an underlying absorption edge at around 387 nm corresponding to an estimated band gap of 3.09 eV. Upon doping with Zn, the absorption edge shifted significantly, extending into the visible light region, which resulted in a reduction of the band gap. Specifically, for Zn concentrations of 1-5 wt.% the band gap decreased from 3.09 eV for undoped TiO_2 to 2.93 eV for 4% Zn-doped TiO_2 and at 2.97 eV for 5% Zn doping (Fig. 11). Table-1 summarizes the effect of Zn loading on surface area, optical properties, charge recombination behaviour and photocatalytic performance of TiO_2.

Photocatalytic activity performance

Screening of catalysts for spent wash degradation: The photocatalytic performance of undoped TiO_2 and Zn-doped TiO_2 (1-5 wt.%) catalysts was evaluated for the degradation of distillery spent wash under natural sunlight. A control experiment without catalyst was also conducted to examine direct photolysis. In the absence of photocatalyst, colour removal was negligible, with less than 5% degradation after 6 h of sunlight exposure. In contrast, the addition of TiO_2 and Zn-doped TiO_2 catalysts markedly enhanced spent wash decolourisation under solar irradiation.

The degradation efficiency was monitored from the decrease in absorbance of melanoidin at ~275 nm using UV-visible spectroscopy (200-800 nm). Undoped TiO_2 exhibited moderate activity, achieving about 62% colour removal after 6 h. All Zn-doped samples performed better than pure TiO_2, with 4% Zn-TiO_2 showing the highest efficiency of ~78% after 6 h (Fig. 12), whereas the catalysts containing 1-3% Zn showed moderate performance. Fig. 13 illustrates the percentage colour degradation with irradiation time at 1 h intervals.

Using the optimum catalyst, the pH of treated effluent increased from acidic (4.5) to near neutral (7.1), indicating improved suitability for safe disposal. A significant reduction in total dissolved solids (TDS), consistent with COD decrease, suggested decomposition and partial precipitation of

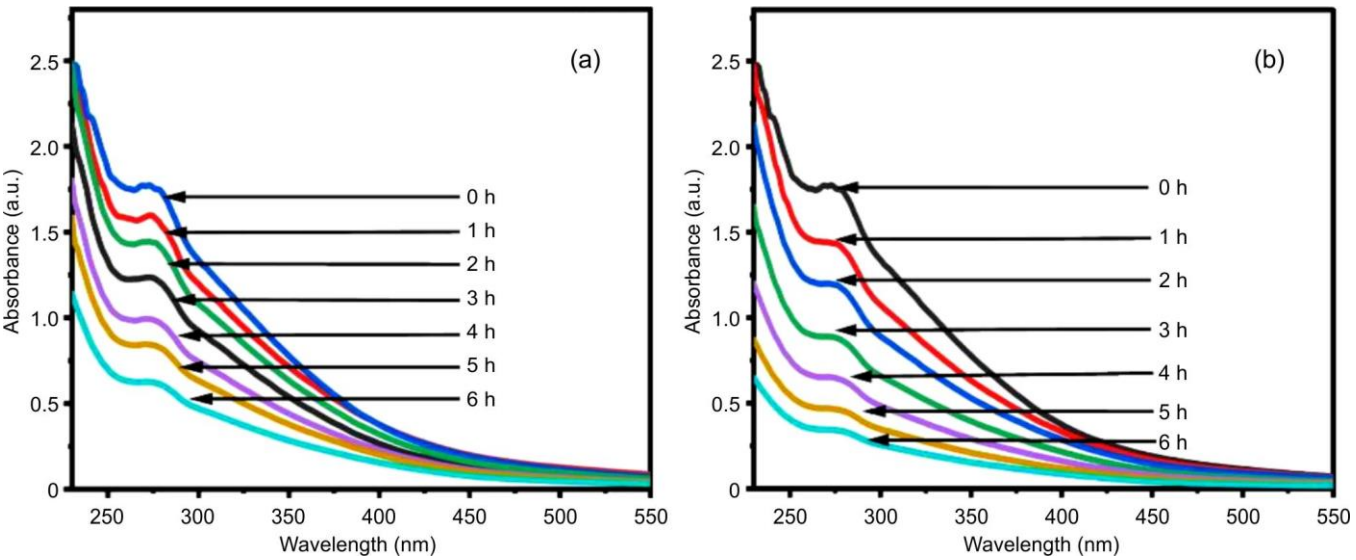

Fig. 12. Photodegradation of spent wash in natural sunlight by using (a) undoped TiO_2, (b) 4% Zn doped TiO_2

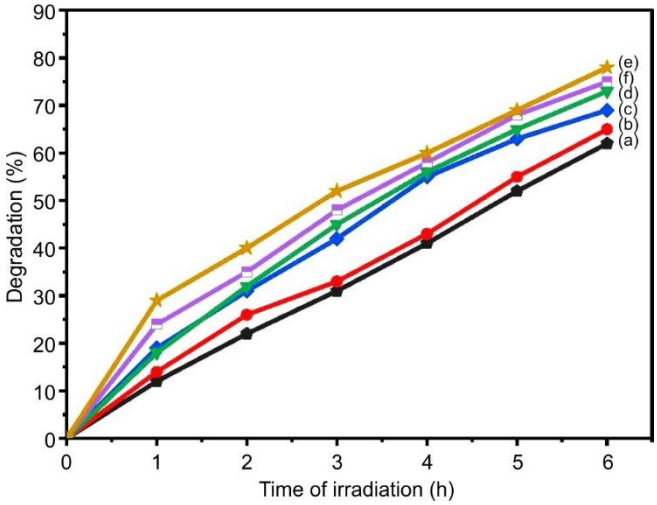

Fig. 13. % Degradation of spent wash after irradiation with natural sunlight using (a) TiO_2, (b) 1% Zn-TiO_2, (c) 2% Zn-TiO_2, (d) 3% Zn-TiO_2, (e) 4% Zn-TiO_2 and (f) 5% Zn-TiO_2

dissolved organic matter. The effect of catalyst dosage was examined at 0.5, 0.75, and 1.0 g/L, where degradation efficiency increased with increasing catalyst loading. The influence of pollutant concentration was also studied at spent wash concentrations of 2500, 5000, 7500 and 10000 mg/L. The colour removal decreased with increasing pollutant concentration due to reduced availability of active sites and higher solution turbidity, which limited light penetration.

Kinetic studies: The photocatalytic degradation of spent wash followed pseudo-first-order kinetics, consistent with the Langmuir-Hinshelwood (L-H) model. The linearised form of the model is expressed as:

$$\ln\left(\frac{C_o}{c}\right) = kt$$

where C_o and C are the initial and final concentration of spent wash; t is the irradiation time and; k is the apparent rate constant. Fig. 14 shows the plot of $\ln(C_o/C)$ *vs.* time. The 4%

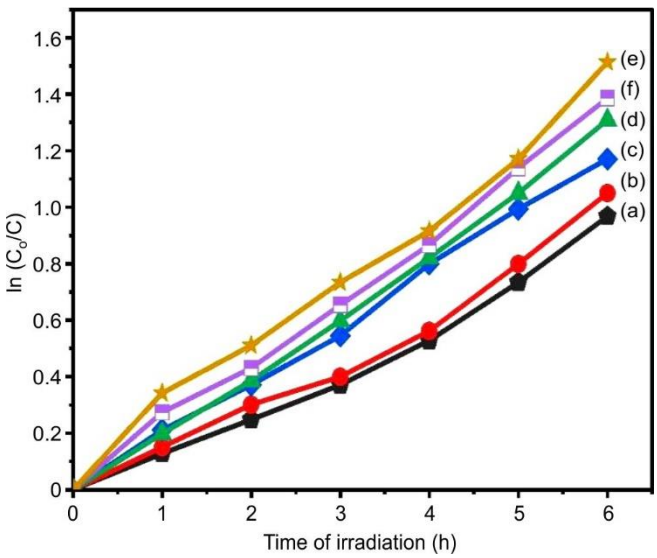

Fig. 14. Rate of degradation of spent wash under natural sunlight by using (a)TiO_2, (b) 1% Zn-TiO_2, (c) 2% Zn-TiO_2, (d) 3% Zn-TiO_2, (e) 4% Zn-TiO_2 and, (f) 5% Zn-TiO_2

Zn-TiO_2 catalyst exhibited the highest rate constant (k = 0.00506 min^{-1}), which is approximately 1.6 times higher than that of undoped TiO_2 (k = 0.00323 min^{-1}). Lower Zn-doped catalysts showed intermediate rate constants, correlating well with their degradation efficiencies. These results confirm that Zn doping enhances charge separation and extends light absorption into the visible region, thereby accelerating the degradation kinetics.

Mineralisation of spent wash: In order to examine complete mineralisation other than only colour removal, COD and TOC values were measured. The COD and TOC removal percentages were ~72% and ~65%, after 6 h of natural sunlight irradiation with 4% Zn-TiO_2, while undoped TiO_2 gave only 56% COD and 52% TOC removals in the same time under similar conditions. These findings reveal that Zn-doped TiO_2 can not only decolourize the spent wash but also convert the organic pollutants into simpler and less toxic molecules, which is true mineralisation. Fig. 15 depicts the suggested photocatalytic degradation pathway of spent wash using Zn-TiO_2 photocatalyst under natural sunlight irradiation.

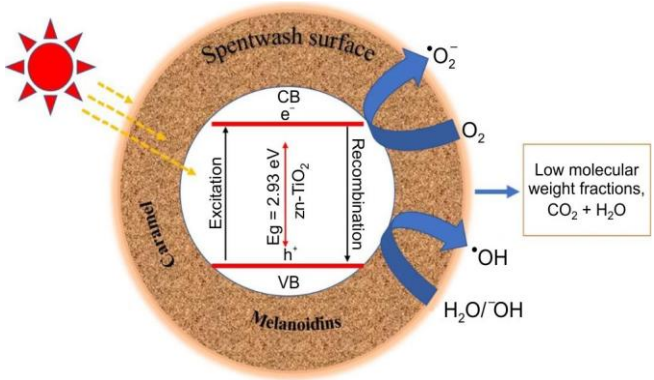

Fig. 15. Schematic representation of the suggested photocatalytic degradation pathway of spent wash over Zn-TiO_2 under natural sunlight

Reusability and stability: The reusability and stability of 4% Zn-TiO_2 were investigated for four consecutive photocatalytic cycles under the same reaction conditions. The catalyst was recovered by centrifugation after each cycle and then washed with distilled water, dried and reused. The degradation efficiency was maintained over 73% after the fourth cycle and decreased only slightly (~5%) relative to the first cycle (78%). XRD analysis of catalysts recovered after four cycles showed that the crystalline phase of the samples was almost unchanged and retained their anatase phase, which exhibited excellent stability and recyclability. The catalyst showed stable photocatalytic performance over repeated cycles, suggesting good structural stability. Although Zn leaching was not quantitatively analysed in the present study, Zn species are expected to be strongly incorporated into the TiO_2 lattice, likely through substitutional doping associated with oxygen vacancies (Zn–O–Ti linkages). Such strong lattice incorporation enhances catalyst stability through stronger bonding interactions, thereby minimizing the potential release of metal ions. Thus, the screening, optimisation and kinetic analyses have proved that 4% Zn-TiO_2 is the best photocatalyst for spent wash degradation due to the synergistic effect of reduced band gap, improved charge separation, higher surface area and stability.

TABLE-2
COMPARATIVE DATA OF DOPED-TiO_2 PHOTOCATALYSTS REPORTED FOR DEGRADATION OF SPENT WASH AND SIMILAR COMPLEX EFFLUENTS

Photocatalyst	Synthesis method	Effluent	Light source	Degradation (%)	Conc. (ppm)	Time (h)	Ref.
Cr-TiO_2	Sol gel	Spent wash	Sunlight	~68–70	10,000	5 h	[27]
V-TiO_2	Sol gel	Spent wash	Sunlight	~65	10,000	5 h	[46]
Cu-TiO_2	Hydrothermal	Spent wash	Sunlight	~59	10,000	5 h	[49]
TiO_2-MoS_2/MXenes	Sol gel	Molasses spent wash (MSW)	300 W Xenon lamp	~85%	10	2 h	[50]
TiO_2/MoS_2	Hydrothermal	Molasses spent wash (MSW)	Sunlight	~72%	25	4 h	[51]

The COD/TOC results confirmed actual mineralisation and the reusability results proved excellent stability of the Zn-doped TiO_2 nanocatalyst. Table-2 compares the photocatalytic performance of the present Zn-TiO_2 system with the previously reported doped-TiO_2 photocatalysts for spent wash and similar complex effluents.

Conclusion

In this study, Zn-doped TiO_2 nanocatalysts containing 1-5% Zn were successfully synthesized by a simple and cost-effective sol-gel method. Zn^{2+} ions were effectively incorporated into the TiO_2 lattice without formation of secondary ZnO phases, resulting in lattice distortion, increased surface area and improved optical properties. The band gap decreased from 3.09 eV for undoped TiO_2 to 2.93 eV for 4% Zn-TiO_2, extending light absorption into the visible region. Photoluminescence studies showed that 4% Zn doping most effectively suppressed electron-hole recombination, while BET analysis confirmed a higher specific surface area with more active sites. Zn doping significantly enhanced the photocatalytic degradation of distillery spent wash under sunlight. Among all samples, 4% Zn-TiO_2 showed the best performance, achieving about 78% colour removal along with 72% COD and 65% TOC reduction within 6 h. The degradation followed pseudo-first-order kinetics, with a rate constant 1.6 times higher than that of undoped TiO_2. The improved activity is attributed to better charge separation, extended light absorption and larger surface area. The catalyst also exhibited good stability, retaining high activity after four reuse cycles without major structural changes. Based on this, 4% Zn-TiO_2 nanocatalyst is found an efficient, stable and recyclable solar-driven photocatalyst, offering a practical and eco-friendly approach for treatment of recalcitrant distillery wastewater.

ACKNOWLEDGEMENTS

The authors are grateful to Department of Chemistry, Annasaheb Magar Mahavidyalay Hadapsar, Pune & Vidya Pratishthan's Supe Arts Science and Commerce College Supe, Tal. Baramati, Pune, India for providing the necessary research resources and facilities to conduct this research.

CONFLICT OF INTEREST

The authors declare that there is no conflict of interests regarding the publication of this article.

DECLARATION OF AI-ASSISTED TECHNOLOGIES

During the preparation of this manuscript, the authors used an AI-assisted tool(s) to improve the language. The authors reviewed and edited the content and take full responsibility for the published work.

REFERENCES

1. V. Kumar, R. Chandra, I.S. Thakur, G. Saxena and M.P. Shah, in eds.: M. Shah and A. Banerjee, Recent Advances in Physicochemical and Biological Treatment Approaches for Distillery Wastewater, In: Combined Application of Physico-Chemical & Microbiological Processes for Industrial Effluent Treatment Plant, Singapore: Springer, 2020.; https://doi.org/10.1007/978-981-15-0497-6_6
2. S. Mohana, B. K. Acharya and D. Madamwar, *J. Hazard. Mater.*, **163**, 12 (2009); https://doi.org/10.1016/j.jhazmat.2008.06.079
3. S. Kumari, K. Yadav and S. Jagadevan, in eds.: I. Haq, A.S. Kalamdhad and S. Dash, Wastewater Treatment and Resource Recovery *via* Struvite Precipitation from High Strength Industrial Wastewater, In: Environmental Degradation: Monitoring, Assessment and Treatment Technologies, Springer, Cham (2022); https://doi.org/10.1007/978-3-030-94148-2_6
4. P. Chowdhary, A. Raj and R.N. Bharagava, *Chemosphere*, **194**, 229 (2018); https://doi.org/10.1016/j.chemosphere.2017.11.163
5. C. Naveen, P. K. Ghodke, A. K. Sharma and W.-H. Chen, *Environ. Technol. Innov.*, **31,** 103202 (2023); https://doi.org/10.1016/j.eti.2023.103202
6. D. Pant and A. Adholeya, *Bioresource Technol.*, **98,** 2321 (2007); https://doi.org/10.1016/j.biortech.2006.09.027
7. W. Mikucka and M. Zielińska, *Appl. Biochem. Biotechnol.*, **192**, 770 (2020); https://doi.org/10.1007/s12010-020-03343-5
8. C. David, M. Arivazhagan and F. Tuvakara, *Ecotoxicol. Environ. Saf.*, **121**, 142 (2015); https://doi.org/10.1016/j.ecoenv.2015.04.038
9. U. Hübner, S. Spahr, H. Lutze, A. Wieland, S. Rüting, W. Gernjak and J. Wenk, *Heliyon*, **10**, e30402 (2024); https://doi.org/10.1016/j.heliyon.2024.e30402
10. S. Banerjee, S.C. Pillai, P. Falaras, K.E. O'Shea, J.A. Byrne and D.D. Dionysiou, *J. Phys. Chem. Lett.*, **5**, 2543 (2014); https://doi.org/10.1021/jz501030x
11. M.K. Hossain, M.M. Hossain and S. Akhtar, *ACS Omega*, **8**, 1979 (2023); https://doi.org/10.1021/acsomega.2c05107
12. S.M. Gupta and M. Tripathi, *Chinese Sci. Bull.*, **56**, 1639 (2011); https://doi.org/10.1007/s11434-011-4476-1
13. K. Ozawa, M. Emori, S. Yamamoto, R. Yukawa, S. Yamamoto, R. Hobara, K. Fujikawa, H. Sakama and I. Matsuda, *J. Phys. Chem. Lett.*, **5**, 1953 (2014); https://doi.org/10.1021/jz500770c
14. X. Yue, S. Jiang, L. Ni, R. Wang, S. Qiu and Z. Zhang, *Chem. Phys. Lett.*, **615**, 111 (2014); https://doi.org/10.1016/j.cplett.2014.09.054
15. S. Gonuguntla, R. Kamesh, U. Pal and D. Chatterjee, *J. Photochem. Photobiol. C: Photochem. Rev.*, **57**, 100621 (2023); https://doi.org/10.1016/j.jphotochemrev.2023.100621
16. R.A. Husna, Suherman and T.A. Natsir, *Results Eng.*, **19**, 101253 (2023); https://doi.org/10.1016/j.rineng.2023.101253
17. A. Aljaafari, *Curr. Nanoscience*, **18**, 499 (2022); https://doi.org/10.2174/1573413717666210706115018
18. A. Anson-Casaos, C. Martinez-Baron, S. Angoy-Benabarre, J. Hernandez-Ferrer, A.M. Benito, W.K. Maser and M.J. Blesa, *J. Electroanal. Chem.*, **929**, 117114 (2023); https://doi.org/10.1016/j.jelechem.2022.117114

19. Y. Du, X. Niu, X. He, K. Hou, H. Liu and C. Zhang, *Molecules*, **26**, 6031 (2021); https://doi.org/10.3390/molecules26196031
20. M. Kunnamareddy, R. Rajendran, M. Sivagnanam, R. Rajendran and B. Diravidamani, *J. Inorg. Organomet. Polym. Mater.*, **31**, 2615 (2021); https://doi.org/10.1007/s10904-021-01914-5
21. S. Du, J. Lian and F. Zhang, *Trans. Tianjin Univ.*, **28**, 33 (2022); https://doi.org/10.1007/s12209-021-00303-w
22. S. S. Ghumro, B. Lal and T. Pirzada, *ACS Omega*, **7**, 4333 (2022); https://doi.org/10.1021/acsomega.1c06112
23. R. A. Rescigno, O. Sacco, V. Venditto, A. Fusco, G. Donnarumma, M. Lettieri, R. Fittipaldi and V. Vaiano, *Photochem. Photobiol. Sci.*, **22**, 1223 (2023); https://doi.org/10.1007/s43630-023-00363-y
24. B.-G. Park, *Gels*, **8**, 14 (2022); https://doi.org/10.3390/gels8010014
25. G.S. Waweru, S. Kiprotich and P. Waithaka, *Adv. Mater.*, **13**, 20 (2024); https://doi.org/10.11648/j.am.20241302.11
26. T. Raguram and K. Rajni, *Int. J. Hydrogen Energy*, **47**, 4674 (2022); https://doi.org/10.1016/j.ijhydene.2021.11.113
27. S.P. Takle, O.A. Apine, J.D. Ambekar, S.L. Landge, N.N. Bhujbal, B.B. Kale and R.S. Sonawane, *RSC Adv.*, **9**, 4226 (2019); https://doi.org/10.1039/C8RA10026H
28. L. Rossi, M. Palacio, P.I. Villabrille and J.A. Rosso, *Environ. Sci. Poll. Res.*, **28**, 24112 (2021); https://doi.org/10.1007/s11356-021-12339-5
29. R.J. Kamble, P.V. Gaikwad, K.M. Garadkar, S.R. Sabale, V.R. Puri and S.S. Mahajan, *J. Iran. Chem. Soc.*, **19**, 303 (2022); https://doi.org/10.1007/s13738-021-02303-y
30. W. Choi, A. Termin and M.R. Hoffmann, *J. Phys. Chem.*, **98**, 13669 (1994); https://doi.org/10.1021/j100102a038
31. R. Dholam, N. Patel, M. Adami and A. Miotello, *Int. J. Hydrogen Energy*, **34**, 5337 (2009); https://doi.org/10.1016/j.ijhydene.2009.05.011
32. H. Irie, K. Kamiya, T. Shibanuma, S. Miura, D.A. Tryk, T. Yokoyama and K. Hashimoto, *J. Phys. Chem. C*, **113**, 10761 (2009); https://doi.org/10.1021/jp903063z
33. R. Janisch, P. Gopal and N. A. Spaldin, *J. Phys.: Condens. Matter*, **17**, R657 (2005); https://doi.org/10.1088/0953-8984/17/27/R01
34. Y. Yu, J. Wang, W. Li, W. Zheng and Y. Cao, *CrystEngComm*, **17**, 5074 (2015); https://doi.org/10.1039/C5CE00933B
35. T. Munir, A. Mahmood, N. Abbas, A. Sohail, Y. Khan, S. Rasheed and I. Ali, *ACS Omega*, **9**, 34841 (2024); https://doi.org/10.1021/acsomega.4c04183
36. K. Santhi, S. Ponnusamy, S. Harish and M. Navaneethan, *J. Mater. Sci.: Mater. Electr.*, **33**, 9798 (2022); https://doi.org/10.1007/s10854-022-07945-z
37. R. Y. Iskra and R. S. Fedoruk, *Physiol. J./Fiziol. Zh.*, **68**, 89 (2022); https://doi.org/10.15407/fz68.04.089
38. M. Pelaez, N.T. Nolan, S.C. Pillai, M.K. Seery, P. Falaras, A.G. Kontos, P.S.M. Dunlop, J.W.J. Hamilton, J.A. Byrne, K. O'Shea, M.H. Entezari and D.D. Dionysiou, *Appl. Catal. B: Environ.*, **125**, 331 (2012); https://doi.org/10.1016/j.apcatb.2012.05.036
39. I. Elmehasseb, S. Kandil and K. Elgendy, *Optik*, **213**, 164654 (2020); https://doi.org/10.1016/j.ijleo.2020.164654
40. R. Ratshiedana, O.J. Fakayode, A.K. Mishra and A.T. Kuvarega, *J. Water Process Eng.*, **44**, 102372 (2021); https://doi.org/10.1016/j.jwpe.2021.102372
41. K. Prajapat, U. Mahajan, M. Dhonde, K. Sahu and P.M. Shirage, *Chem. Phys. Impact*, **8**, 100607 (2024); https://doi.org/10.1016/j.chphi.2024.100607
42. A. Ribeiro, M. Proença, N. Catarino, M. Dias, M. Peres, J. Borges, F. Vaz and E. Alves, *Nucl. Instrum. Methods Phys. Res. B*, **541**, 336 (2023); https://doi.org/10.1016/j.nimb.2023.05.068
43. O. Sadek, S. Touhtouh, M. Rkhis, R. Anoua, M. El Jouad, F. Belhora and A. Hajjaji, *Mater. Today: Proc.*, **66,** 456 (2022); https://doi.org/10.1016/j.matpr.2022.06.385
44. D. V. Aware and S. S. Jadhav, *Appl. Nanosci.*, **6**, 965 (2016); https://doi.org/10.1007/s13204-015-0513-8
45. Y. Yu, J. Wang, W. Li, W. Zheng and Y. Cao, *CrystEngComm*, **17**, 5074 (2015); https://doi.org/10.1039/C5CE00933B
46. S.P. Takle, S.D. Naik, S.K. Khore, S.A. Ohwal, N.M. Bhujbal, S.L. Landge, B.B. Kale and R.S. Sonawane, *RSC Adv.*, **8**, 20394 (2018); https://doi.org/10.1039/C8RA02869A
47. B. D. Cullity and R. Smoluchowski, *Physics Today*, **10**, 50 (1957); https://doi.org/10.1063/1.3060306
48. Y. Masuda and K. Kato, *J. Ceramic Soc. Japan*, **117**, 373 (2009); https://doi.org/10.2109/jcersj2.117.373
49. S.P. Takle, O.A. Apine, D.B. Bankar, A.S. Tarlekar, N.N. Bhujbal, B.B. Kale and R.S. Sonawane, *New J. Chem.*, **44**, 17724 (2020); https://doi.org/10.1039/D0NJ03309J
50. N. Khan, M. B. Tahir, B. Ahmed and M. Sagir, *J. Electr. Mater.*, **54**, 7038 (2025); https://doi.org/10.1007/s11664-025-12114-z
51. N. Khan, M. B. Tahir, B. Ahmed and M. Sagir, *Emer. Mater.*, **8**, 5703 (2025); https://doi.org/10.1007/s42247-025-01150-4